Construction and Building Materials 126 (2016) 894–912

Contents lists available at ScienceDirect

Construction and Building Materials

journal homepage: www.elsevier.com/locate/conbuildmat

Evaluating the early-age behaviour of full-scale prestressed concrete beams using distributed and discrete fibre optic sensors

Liam J. Butler [a,*], Niamh Gibbons [a], Ping He [b], Campbell Middleton [a], Mohammed Z.E.B. Elshafie [a]

[a] Department of Engineering, University of Cambridge, UK
[b] Department of Geotechnical Engineering, Tongji University, China

HIGHLIGHTS

- Distributed and discrete fibre optic sensors were installed in prestressed beams.
- Strain data were recorded during beam manufacturing and over the first 6 months.
- Results highlight the effect of beam production on early age prestress losses.
- Measured prestress losses were up to 79% of Eurocode 2 predicted ultimate losses.
- Strain-derived camber at detensioning underestimated theoretical 6 month cambers.

GRAPHICAL ABSTRACT

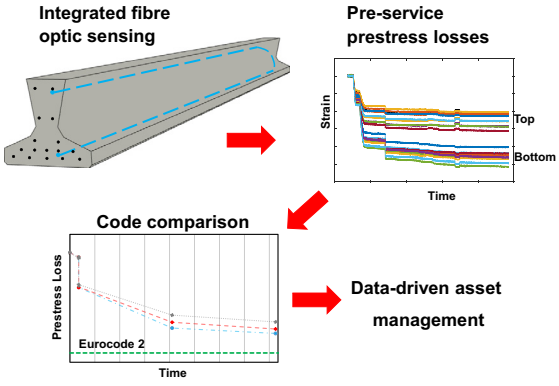

ARTICLE INFO

Article history:
Received 26 June 2016
Received in revised form 16 September 2016
Accepted 21 September 2016

Keywords:
Fibre optics
Prestressed concrete
Railway bridges
Structural health monitoring
Self-sensing structures

ABSTRACT

This paper evaluates the results of a monitoring study that captures the early age behaviour of four 11.9 m prestressed concrete bridge beams utilising both distributed and discrete fibre optic sensor (FOS) arrays. The performance of the beams is evaluated before they are placed in-service as part of new concrete railway bridges in the Midlands in the UK. Two types of prestressed beams were monitored, two TY7 internal beams and two TYE7 edge beams. The beams incorporated high strength (up to 90.7 MPa) self-consolidating concrete. The entire manufacturing process which included early-age curing and the detensioning process was captured in great detail using the installed FOS system. An analysis of the curing strains within the beams revealed the significant effect that ambient temperature, curing duration, and formwork restraint has on the development of prestress losses prior to detensioning. Based on the distributed FOS readings, it was observed that the strain remained uniform along the length of the beams during the various beam monitoring stages. The measured strain data was then used to calculate prestress losses in the first six months after casting (prior to casting of the in-situ concrete bridge deck). The TY7 and TYE7 beams experienced losses that were 79% and 72% of the ultimate losses predicted using Eurocode 2 equations, respectively. Distributed strain measurements were used to provide estimates of the change in beam camber with time. The pre-camber values calculated using the recorded FOS strain data at the time of detensioning closely match the theoretically calculated values. However, camber values increased by up to 1.7 times in the first six months compared with the post-detensioning values and deviated significantly from the theoretically calculated values. The future aim of this research is to establish integrated FOS systems as viable tools for monitoring strain evolution in concrete bridges in

* Corresponding author.
E-mail address: LB643@cam.ac.uk (L.J. Butler).

http://dx.doi.org/10.1016/j.conbuildmat.2016.09.086
0950-0618/

order to establish comprehensive baselines to facilitate long term data-driven bridge monitoring programmes.

1. Introduction and Background

During recent decades, fibre optic sensors (FOS) have been used increasingly to monitor the changing condition of a variety of infrastructure assets around the world. In many cases, the assets are instrumented because they are critical or landmark structures (i.e., dams, landmark bridge structures, power plants, etc.) or because their existing and/or remaining capacity has been called into question (i.e., old bridges, deteriorating buildings, historically valuable assets, etc.). As a result, the use of FOS technology has primarily been limited to one-off type applications and often times is not installed during the construction phases of a structure. There is however, a greater potential to impact the entire life cycle of an infrastructure asset through the widespread installation of FOS networks in new structural components. These components could be manufactured either on or off-site and would consist of primary load-bearing elements such as piles, footings, columns, slabs or beams. Permanently integrating FOS into one or more of these critical elements before they are placed in service allows the entire load history of these elements to be captured over time. In the case of modular structural components, invaluable information can be gathered to help manufacturers optimise their processes. Therefore, engineers and researchers can assess design assumptions against measurements of real behaviour and asset managers can more confidently address future questions about an assets' existing and/or remaining capacity and its potential for reuse in other structures. In particular, prestressed concrete beams are ideal candidates for being converted into 'self-sensing' structural elements as they are often produced in controlled conditions in which sensor instrumentation could be added to the manufacturing process; and, because their behaviour changes significantly with time, having a means to measure these changes accurately is invaluable.

Research into the time-dependent behaviour of precast prestressed concrete beams has been ongoing for several decades. Prestressed concrete offers many advantages over reinforced concrete in terms of controlling cracking and minimising long-term deflections. In addition, by using high strength self-consolidating concrete (SCC) mixtures, the overall constructability and quality of the finished product can be greatly improved. The use of high strength concrete in bridge beams offers economic advantages over traditional mixes due to increased stiffness and reduced deflections, permitting longer spans and smaller section sizes. However, accurate prediction of the prestress losses in high-strength concrete, in particular at an early age, is required for design. An underestimation of the prestress losses may lead to cracking under service conditions and an associated reduction in section efficiency which can lead to long term durability issues. In contrast, overestimating prestress losses in a beam can lead to excessive camber and unnecessary additional elastic shortening. Therefore, it is important to provide accurate prestress loss predictions to ensure that the remaining prestressing force is adequate to control deflections of prestressed members under permanent load. Guidance in current European (EN 1992-1-1:2004) [1] and American (AASHTO-LRFD) [2] standards pertaining specifically to high strength concrete is limited and has been identified as an area requiring further investigation [3]. Calculating reasonable estimates of early age prestress losses in prestressed beams that use high strength SCC before they are made composite with the concrete bridge deck has also not been studied extensively. There have been several experimental studies that have investigated quantifying early age time-dependent behaviour in prestressed concrete beams. A large study was conducted by Garber et al. [4] on 30 full-scale precast prestressed bridge beams with the aim of measuring prestress losses for up to three years. The beams were 13.9 m long AASHTO Type C I-beams of two different depths, 1016 mm and 1168 mm. Vibrating wire strain gauges were used to validate a flexural service load testing method for estimating long-term prestress losses. Examining the prestress losses that occurred during the first year, it was found that 90% of the 1 year prestress loss took place within the first 4 months and that the prestress losses were highly influenced by the concrete stiffness properties. Porco et al. [5] attached SOFO (*Surveillance d'Ouvrages par Fibres Optiques*) sensors directly to the prestressing strands of eight prestressed concrete beams that formed the superstructure of a simply supported bridge viaduct in Bari, Italy. The prestress in the strands were monitored during several stages of construction including after detensioning of the strands, after casting of the concrete deck slab, and after the permanent dead loads were in place. It was found that the measured prestress losses were 4–24% lower that the losses predicted using Eurocode 2 [1]. Lin et al. [6] conducted laboratory testing of post-tensioned concrete beams with embedded fibre Bragg grating (FBG) fibre optic sensors. The thermal strains due to concrete curing and the mechanical strains induced during the post-tensioning process were measured. In addition, a method for detecting crack locations and depths when the beams were subjected to four-point bending stresses was established. Khayat and Mitchell [7] investigated the structural performance of four full-scale AASHTO Type II precast pretensioned beams constructed using SCC. Using embedded vibrating wire strain gauges, it was identified that the SCC mixtures developed higher autogenous shrinkage in the first 28 days and higher drying shrinkage and creep strains in the first 300 days compared to the control beams. The authors concluded that due to the greater drying shrinkage values, SCC beams may experience higher prestress losses and smaller camber values.

In reviewing a broad range of studies in field monitoring of prestressed concrete beams, to the Authors current knowledge, there have been no studies that have integrated both distributed and discrete fibre optic sensors at the time of manufacture to measure the early age behaviour of prestressed concrete beams. In addition, there appears to be a need to compare field measured values of early-age prestress losses to those predicted based on the Eurocode 2 equations. Depending on the age of the beams when they are placed in service (i.e., installed on the bridge abutments and after the concrete deck is cast), this could have a significant effect on their prestress losses and subsequent in-service behaviour because of the differential creep and shrinkage that occurs within the beams and in-situ concrete deck.

This study investigates the pre-service behaviour (i.e., prior to casting compositely with the concrete bridge deck) of four newly constructed prestressed concrete beams that form part of the superstructure of a new 11.2 m concrete railway bridge near Stafford UK. The construction of this bridge is part of a large rail infrastructure upgrade and redevelopment scheme known as the Stafford Area Improvements Programme [8].

This study is significant as it presents an integrated FOS system for mass-produced prestressed concrete beams. Both discrete fibre Bragg grating based sensors that can measure dynamic strain and distributed fibre optic sensors based on Brillouin Optical Time Domain Reflectometry that measure strain along a prestressing

strand at 5 cm intervals have been installed in all four beams. By using these two types of sensors in combination, this study represents a first in measuring in unprecedented detail, the early-age time-dependent distributed strain changes experienced by pre-stressed beams. By using distributed sensing systems, the deflected shape and pre-camber along the length of the beams can be calculated using elastic beam theory. Presenting monitoring data in the context of these performance parameters greatly increases the value of this type of data and allows asset operators to make better informed decisions. Finally, this study provides a highly characterised pre-service baseline for measuring critical performance parameters throughout the life of the structure. Having detailed and reliable structural performance data for new structures can help inform asset managers and engineers in planning maintenance and inspection regimes and in evaluating the remaining capacity of an asset.

2. Fibre optic sensor technology

The use of FOS for monitoring civil infrastructure has been ongoing for the past two decades. However, its widespread adoption in routine monitoring practice, particularly in the monitoring of new structures is still relatively uncommon. There are a variety of FOS types and configurations available through a wide range of manufacturers operating around the world. They can be used to measure a variety of different parameters such as strain, temperature, vibration, and acceleration. In general, FOS offer several advantages over conventional sensors including being relatively small and lightweight, resistant to corrosion and electromagnetic interference, and readily embeddable into structural materials [9]. FOS can be generally divided into two categories: distributed and discrete. Distributed FOS such as those based on Brillouin Optical Time Domain Reflectometry (BOTDR) can measure strain statically along the entire length of a fibre optic cable. Discrete or point-based FOS such as those based on fibre Bragg gratings (FBG) measure strain dynamically at specific locations. When used in combination, these systems can provide a highly detailed strain profile of a structural element. The following sections describe the physical principles of each sensor technology.

2.1. Brillouin optical time domain reflectometry

The glass core in fibre optic cables has an amorphous structure that results in the scattering of light signals sent through them. In telecommunications, this causes attenuation of the useful signal, but it is precisely this effect that can be exploited when using fibre optic cables to collect strain and temperature data. The scattered light can be divided into three main modes known as, Rayleigh, Brillouin, and Raman scattering. In general, Brillouin backscattered light arises as a result of density changes in the glass medium of the core which causes a phonon wave to travel through the medium. The frequency at which the backscattered signal is most intense is known as the Brillouin frequency. By finding the Brillouin frequency information, the local density is known. This can be related to the local temperature and to local strain using Eq. (1),

$$\nu_b(s) = \nu_{bo} + M\varepsilon(s) \tag{1}$$

where $\nu_b(s)$ is the Brillouin frequency shift as a function of distance; ν_{bo} is the Brillouin shift with zero induced strain; M is a constant of proportionality; and $\varepsilon(s)$ is the thermal/mechanically induced strain as a function of distance.

As Brillouin-based measurements detect shifts in frequency rather than the intensity of the backscattered signals, they allow for measurements over spans greater than 10 km [10–12]. Having established that it is possible to determine local properties such as ambient temperature or strain, these can then be combined to create a complete temperature or strain profile along the cable. Decoupling of the strain and temperature effects is achieved by having the optic fibre cores separated from the protective rubber casing of the cable by a gel layer, and isolating them from the external strains applied to the cable.

2.2. Fibre Bragg gratings

A fibre Bragg grating (FBG) is a periodic refractive index variation constructed in a short segment of optical fibre core by exposing the fibre to an ultraviolet interference pattern. The FBG reflects particular wavelengths of light and transmits all others [13–16]. The reflected wavelength has a very small bandwidth which is shown as a peak in the spectrum. A series of gratings can be inscribed on a single fibre; with each grating manufactured with a unique period that will have a signature base wavelength corresponding to the period of the index of refraction variation of the FBG.

FBGs are known to have a stable and reliable wavelength response as a function of the applied strain. Straining an FBG sensor causes a change in the grating period resulting in a change in the wavelength of the reflected ultraviolet light. Due to the temperature and strain dependence of the refractive index of glass and grating period of the FBG, the wavelength of the reflected component will also change as function of both temperature and/or strain. The relationship between the change in the wavelength and the base wavelength is shown in Eq. (2) below, and is dependent on the input mechanical strain, temperature induced strain in the substrate and the change in the refractive index of the glass due to temperature [17].

$$\frac{\Delta\lambda}{\lambda_o} = k(\varepsilon_m + \alpha_{sp} * \Delta T) + \alpha_\delta * \Delta T \tag{2}$$

where

$\Delta\lambda$ = measured change in wavelength of FBG
λ_o = base wavelength of FBG
k = gauge factor; typical value = 0.78
ε_m = mechanical strain applied to the fibre
α_{sp} = expansion coefficient of the substrate material (e.g., concrete) (K^{-1})
ΔT = change in temperature (K)
α_δ = change in the refractive index (K^{-1}); typical values between 5 and 8×10^{-6}.

As a result of the temperature dependence of the FBG output, precise strain measurements can only be achieved with careful temperature compensation. This can be achieved either by fixing an FBG to a position without mechanical strain and/or by measuring the temperature directly with a pure temperature measuring FBG. The calculation of the mechanical strain is calculated using Eq. (3) for use with a temperature compensating FBG [17].

$$\varepsilon_m = \frac{1}{k}\left(\frac{\Delta\lambda_m}{\Delta\lambda_{om}} - \frac{\Delta\lambda_c}{\Delta\lambda_{oc}}\right) \tag{3}$$

where,

$\Delta\lambda_m$ = wavelength shift of strain-measuring FBG
$\Delta\lambda_{om}$ = base wavelength of strain-measuring FBG
$\Delta\lambda_c$ = wavelength shift of temperature compensation FBG
$\Delta\lambda_{oc}$ = base wavelength of temperature compensation FBG.

2.3. Fibre optic sensors used in this study

Both strain FBGs and temperature compensating FBGs were used in order to measure the mechanical strains developed within the beams. BOTDR cables consisted of reinforced single mode fibre

(4 mm diameter) which was sufficiently robust to be used as its own routing cable. Unlike the FBG sensors, the BOTDR cables can only measure static changes in strain. The strain measuring FBGs used in this study were produced by FBGS Technologies and contain 20 FBGs per sensor array spaced at one metre and can measure strain changes within ±5 με. The manufacturing process for these FBGs is unique in that the gratings are created during the drawing of the glass fibre and prior to the application of protective coating; these are referred to as Draw Tower Gratings (DTGs). FBGs manufactured by this process have several distinct advantages over traditionally recoated FBGs: 1) they have superior mechanical tensile strength, 2) an array of FBGs can be created on one continuous fibre eliminating the need for splicing multiple separate FBGs, and 3) have a relatively lower cost compared to traditional FBG sensors. To provide additional durability and strength during the installation process, these FBGs were manufactured using low bend loss fibre and with an additional glass fibre reinforced polymer (GFRP) coating (2 mm diameter). In order to provide additional length of cable for routing to the fibre optic analysers, a reinforced single-mode fibre cable (5 mm diameter) was spliced to the end of the FBG cable prior to exiting the ends of the beams. Temperature compensation for both FBG and BOTDR strain measurements was performed using FBG point-based temperature sensors manufactured by Micron Optics. Each array contained six FBG temperature sensors with a temperature accuracy of ±1.0 °C and was packaged in a 1 mm fibreglass braided cable.

3. Sensor arrangements and installation

The following section presents the sensor installation procedures as they relate to the various stages of beam fabrication and installation. A total of six prestressed concrete beams were instrumented with both distributed (BOTDR) and discrete (FBG) fibre optic sensors. However, only data from four of the beams are presented in this study as they were monitored during the entire fabrication process. Two beams were TY7-type beams (referred to as BM2 and BM3) and the remaining two were edge TYE7-type beams (referred to as BM1 and BM9). Fig. 1 depicts the beam dimensions and sensor layout patterns for both the internal TY7 and edge TYE7 beams.

As shown in Fig. 1, and 20 FBG strain sensors, 6 FBG temperature compensating sensors, and 22 m of BOTDR strain sensor cable were installed in each of the beams. The sensor cables were installed to the underside of the prestressing strands (refer to Fig. 1) using plastic cable ties. It should be noted that two of the 19 strands in the TYE7 beams were de-bonded along a 1.5 m length at the each end of the beam, as shown in Fig. 1. The FBG sensors were not installed within this region or along the strands which were de-bonded. In addition, as depicted in Fig. 3(c), the tendon arrangement for the TYE7 beams was asymmetrical. However, sensors were arranged in the horizontal plane only, as the stresses and strains about the strong axis of the section were assumed to be most significant and therefore most critical to measure. In addition,

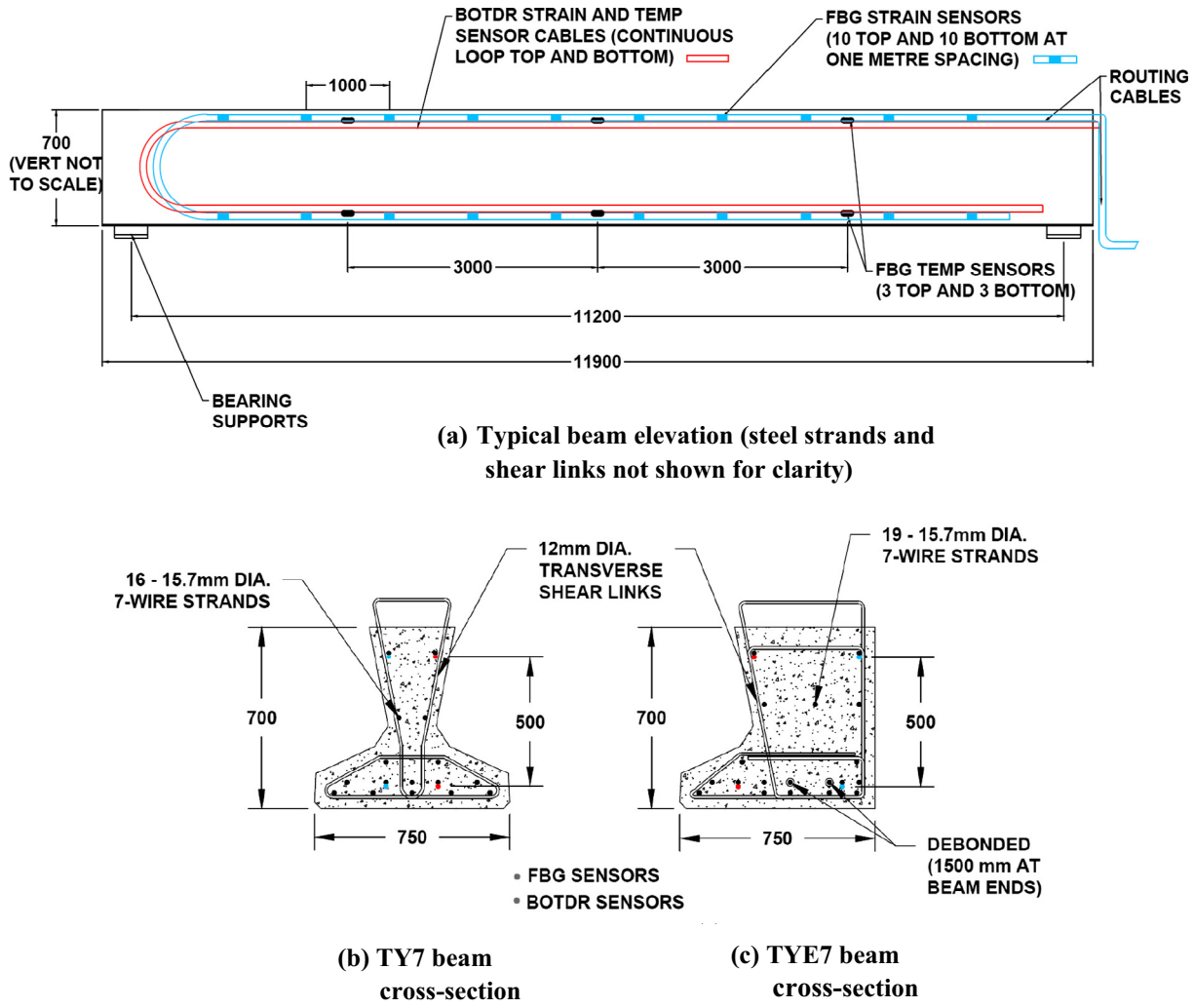

Fig. 1. Typical fibre optic sensor arrangement along prestressed beam.

Fig. 2. Installation of fibre optic sensors on beam reinforcing cages.

Fig. 3. Completed TY7 beams (left) and TYE7 beams (right). Note the sensor cable ends and connectors stored within temporary enclosures.

FBG sensors were installed outside of the transmission zone and dispersion length (i.e. outside of the area of non-linear stress distribution) on both sets of TY7 and TYE7 beams.

Due to both space restrictions within the prestressing yard and the limited channel capacity of the fibre optic analysers, only two of the internal TY7 beams (BM2 and BM3) and two of the external TYE7 beams (BM1 and BM9) could be monitored during the beam manufacturing stages. Subsequent readings were then taken at several stages for the remaining two instrumented beams, i.e., one at approximately 3 months following beam casting and one at approximately 6 months following casting just prior to casting of the concrete bridge deck. Figs. 2 and 3 show the instrumentation of the beams and the completed beams, respectively.

Separate analysers were used for the BOTDR and FBG sensors. A Neubrescope NBX-5000 fibre optic analyser was used to interrogate the distributed strain values measured with the BOTDR cables. The FBG sensors were interrogated using a Micron Optics sm130 dynamical optical sensing interrogator which allowed data to be acquired at up to 1000 Hz. Both analysers were used when recording data at various fabrication stages.

4. Monitoring programme

The overall monitoring programme can be summarised in five separate stages as outlined in Table 1. These include readings taken at the various stages of beam fabrication as well as during their storage and immediately following their installation on the bridge abutments. Table 1 also describes the time-dependent effects that were captured as part of the recorded data at each of the monitoring stages.

The beam fabrication took place during January 2015 at Laing O'Rourke's facility at Explore Industrial Park (EIP) in Worksop, UK. Prestressing beds were located outdoors at the side of the facility and all concrete was batched on site directly adjacent to the prestressing operations. Manufacture of the prestressed beams including the installation of the FOS involved several stages:

1) Strands were run through beam end plates and stressed initially to 69 kN (460 MPa) per strand;
2) Strands were stressed to their full design prestress force of 209 kN (1393.3 MPa) per strand followed by installation of the transverse shear links;
3) Both the BOTDR and FBG fibre optic sensor cables were installed along the top and bottom prestressing strands (refer to Fig. 1);
4) All fibre optic cables were tested and baseline strain readings were recorded prior to concrete casting;
5) Beam shutters (formwork) were installed;
6) Concrete was cast using an overhead crane and hopper system;
7) Chemical set retarding agents were applied to the tops of the beams and they were left to cure in air until they reached adequate compressive strength for detensioning (50 MPa);
8) Beam formwork was removed within the first 73 h after casting;
9) TY7 beams were detensioned in two stages and TYE7 beams were detensioned in a multiple stage process;
10) All excess fibre optic cables and connectors were housed in temporary enclosures prior to removing the beams from the casting beds.

Following manufacture, the beams were transported into a temporary storage area (within EIP) until they were ready to be shipped to the bridge site. Note that in the case of the TYE7 beams,

Table 1
Summary of the various stages of beam monitoring.

Stage	Description	Date(s)				Effects
		TY7 beams (BM2 and BM3)	No. days after casting	TYE7 beams (BM1 and BM9)	No. days after casting	
1	Concrete casting (baseline)	22 Jan 2015	0	9 Jan 2015	0	None prior to concrete initial set
2	Initial curing period prior to transfer of prestress	22–29 Jan 2015	1–7	9–13 Jan 2015	1–3	Initial curing and steel relaxation
3	Pre- and post- transfer of prestress	29 Jan 2015	7	13 Jan 2015	4	Elastic shortening of concrete
3A*	2nd Stage casting	N/A	N/A	5 Mar 2015	55	Added dead load; creep; differential shrinkage
4	Outdoor storage in precast facility (≈3 months)	14 Apr 2015	82	14 Apr 2015	95	Early age steel relaxation, shrinkage and creep
5	Prior to casting of bridge deck (after installation of reinforcing steel and transport of beams)	6 Jul 2015	165	6 Jul 2015	178	Transportation to site and continued steel relaxation, shrinkage and creep

* *Note:* monitoring data was not recorded at the time of this event. Occurred on TYE7 beams only.

they required a second casting whereby an additional 200 mm of concrete was cast along the tops of the beam which formed part of the finished deck slab of the bridge (refer to Stage 3A in Table 1). This second casting took place 55 days following casting of the TYE7 beams however no monitoring data was recorded for this process. Monitoring data was recorded approximately three months after beam casting that included the strain change within the TYE7 beams due to the second casting. All beams were transported to site and were installed on the bridge abutments on June 30th, 2015, approximately 6 months after casting. However, data was not recorded until one week later on July 6th, 2015 (one week prior to casting of the concrete bridge deck).

5. Fibre optic monitoring results and discussion

The following section presents the results recorded from the monitoring of the prestressed beams during their first six months following casting. Both the raw data from the BOTDR cables (central frequency shift) and the FBG sensors (wavelength shift) were converted to mechanical strain (compensated for temperature effects) using the equations presented in Sections 2.1 and 2.2, respectively. Results are presented chronologically beginning with a summary of the tested concrete and prestressing steel properties, the beam manufacturing process which includes the casting, curing and detensioning process of the beams, and then presents the overall strain changes including readings taken at approximately 3 months (storage outdoors in casting yard) and at approximately 6 months (after beams were transported to site and lifted onto the bridge abutments). By recording data at each of these stages, this study presents a detailed evaluation of the internal strain evolution within the beams prior to being placed in service. Note that because the sensors were installed prior to casting of concrete, the strain changes due to self-weight of the beams (directly after detensioning) are captured directly in the measurements.

5.1. Beam fabrication

As described above, the monitoring of the beam fabrication process consisted of several stages: concrete casting, early-age curing, and detensioning of the prestressing strands. The monitoring of the beam fabrication process began during the casting of concrete. All three stages of the beam fabrication process including casting, curing and detensioning were monitored.

It is important to note that the sensors installed within the beams can only measure strain change. That is, they do not give a representation of absolute strain and require that a suitable baseline strain is measured from which further cumulative strains are measured. This study assumes a baseline strain corresponding to the strain reading recorded at one hour after concrete casting. A one hour post-casting baseline was chosen as it was assumed that the concrete had begun to stiffen sufficiently enough such that the embedded fibre optic cables were bonded to the surrounding concrete.

Table 2
Concrete and prestressing steel material properties.

Material property	TY7 beams	TYE7 beams
Casting date	22 Jan 2015	9 Jan 2015
Water/cementitious materials ratio	0.36	0.36
Slump flow	760 mm	770 mm
Design $f_{ck,cube}$ (28 days)	75 MPa	75 MPa
$f_{ck,cube}$ (28 days)‡	89.6 MPa	90.7 MPa
$f_{ck,cube}$ (7 days)‡	75.8 MPa	76.7 MPa
$f_{ck,cube}$ at transfer†	60.5 MPa	65.8 MPa
Estimated E_{cm} at transfer*	35,300 MPa	36,210 MPa
Prestressing steel (7 wire strand)‡‡	16 strands	19 strands
f_{pu}	1860 MPa	1860 MPa
E_p	195,000 MPa	195,000 MPa
ρ_{1000} (elongation after 1000 h)	2.5%	2.5%
A_{strand}	150 mm^2	150 mm^2

‡ Measured values are based on cube specimens cured under controlled conditions, i.e. in water bath.
† Estimate based on measured maturity versus temperature data provided by contractor (detensioning of TYE7 beams occurred 94 h after casting).
* $E_{cm}(1) = (f_{cm}(1)/f_{cm}(28))^{0.3}E_{cm}(28)$; $E_{cm}(28) = 22(f_{cm}(28)/10)^{0.3}$; $f_{ck}(t) = 0.8f_{ck,cube}(t)$.
‡‡ Based on supplier specifications sheets.

The concrete mixture designs for all of the prestressed beams were of strength class C60/75 and were self-compacting, i.e. with slump flows greater than 600 mm. Self-compacting concrete was used to eliminate the need for mechanical consolidation and to attain a higher quality finished concrete surface. The initial prestressing force was assumed to be 209 kN/tendon (1393.3 MPa/strand) based on the nominal design calculations provided by the designer and confirmed by the prestressing facility operators. The concrete and prestressing steel material properties are summarised in Table 2.

5.1.1. Concrete curing

The prestress facility operators monitored concrete maturity using thermocouples installed at the time of concrete casting in order to estimate strength development for determining whether the beams could be detensioned. To achieve a compressive strength of 50 MPa at the time of prestress transfer to the concrete (i.e., detensioning), the internal TY7 beams were cured for 7 days and the TYE7 beams were cured for 3 days. Curing times varied due to the differences in ambient temperature conditions during the two periods of beam fabrication. Recall from Table 1 that the TYE7 beams were cast on 9 January 2015 and the TY7 beams were cast on 22 January 2015. The real-time curing process of all beams

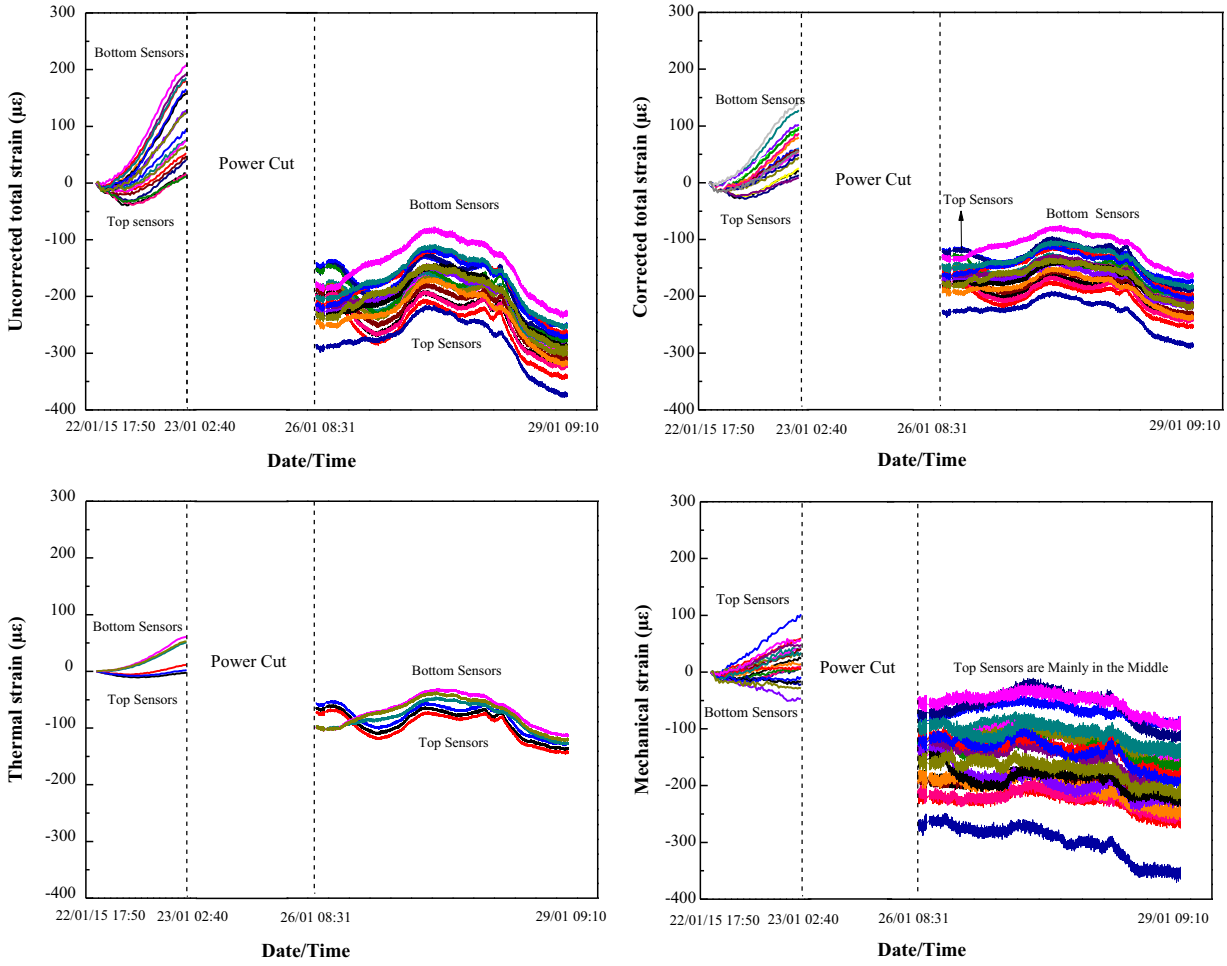

Fig. 4. Recorded mechanical strains during curing of BM2 (baseline = one hour post-casting).

were captured using the FBG sensors and are presented for beams BM2 and BM1 in Figs. 4 and 5, respectively. Note that due to a power outage, a portion of the strain data was not recorded in beam BM2 between approximately 9 and 48 h after casting. In addition, no strain data during the curing process was recorded for BM1 or BM9 due to the malfunction of one of the optical ports on the FBG analyser.

Based on the data presented in Figs. 4 and 5, both BM2 (TY7) and BM1 (TYE7) experienced net positive (tensile) mechanical strain changes during early age hydration and the resulting exothermic reaction. After approximately 9 h, the thermal strains reached their peak values and subsequent concrete shrinkage followed causing net contraction (compression) in the concrete as evidenced by the negative change in mechanical strains. Note that the TY7 beams were demoulded in the early morning of 26/01/2015 and therefore, strain changes within the beam at this time were not recorded due to the power outage.

Although the FBG temperature sensors only provided measures of strain change due to temperature, thermocouples installed by the beam manufacturer were able to provide an absolute measure of temperature. Thermocouples recorded maximum temperatures during curing of approximately 36 °C within the TYE7 beams only, as they malfunctioned during the casting of the TY7 beams. Significant differences in the strains between BM2 (TY7) and BM1 (TYE7) beams were observed during the curing process. This is mainly due to differences in both geometry (mass of concrete and section shape) and ambient conditions as the temperature dropped below 0 °C for the majority of the TY7 beams curing process and precipitation in the form of snow also occurred. These less favourable curing conditions also led to the longer curing period required for the TY7 beams to achieve adequate strength for the transfer of prestress.

In terms of the mechanical strains developed during curing, BM2 (TY7) experienced a net compressive strain as measured by both its top and bottom sensors. These readings confirm the net contraction resulting from concrete autogenous and drying shrinkage. However, after approximately 9 h, BM1 (TYE7) experienced net tension (expansion) in both its top and bottom sensors. As the reported mechanical strains have already accounted for the effects of temperature and thermal strain changes, these strain changes must be due to other mechanisms such as the effect of restraining friction between the bottom of the beam and the casting bed. It is hypothesized that the difference in thermal strains that develop between the top and bottom of the beam after the initial 9 h curing period are restrained by both the forms and casting bed. The bottom of the beam compresses less than that top of the beam due to thermal actions however, the bottom was restrained and therefore an internal moment developed temporarily placing the top of the beam in net tension (approximately 100 με). Similar findings of top expansion and bottom flange restraint were reported by Khayat and Mitchell [7]. A final component of this plot shows a sharp drop in strains at approximately 07:00 on 12/1/15, this corresponded to when the beams were demoulded exposing the concrete surface and rapidly increasing the drying shrinkage (thus causing increased compression). Following this drop, a similar trend was measured whereby a net expansion of the beam

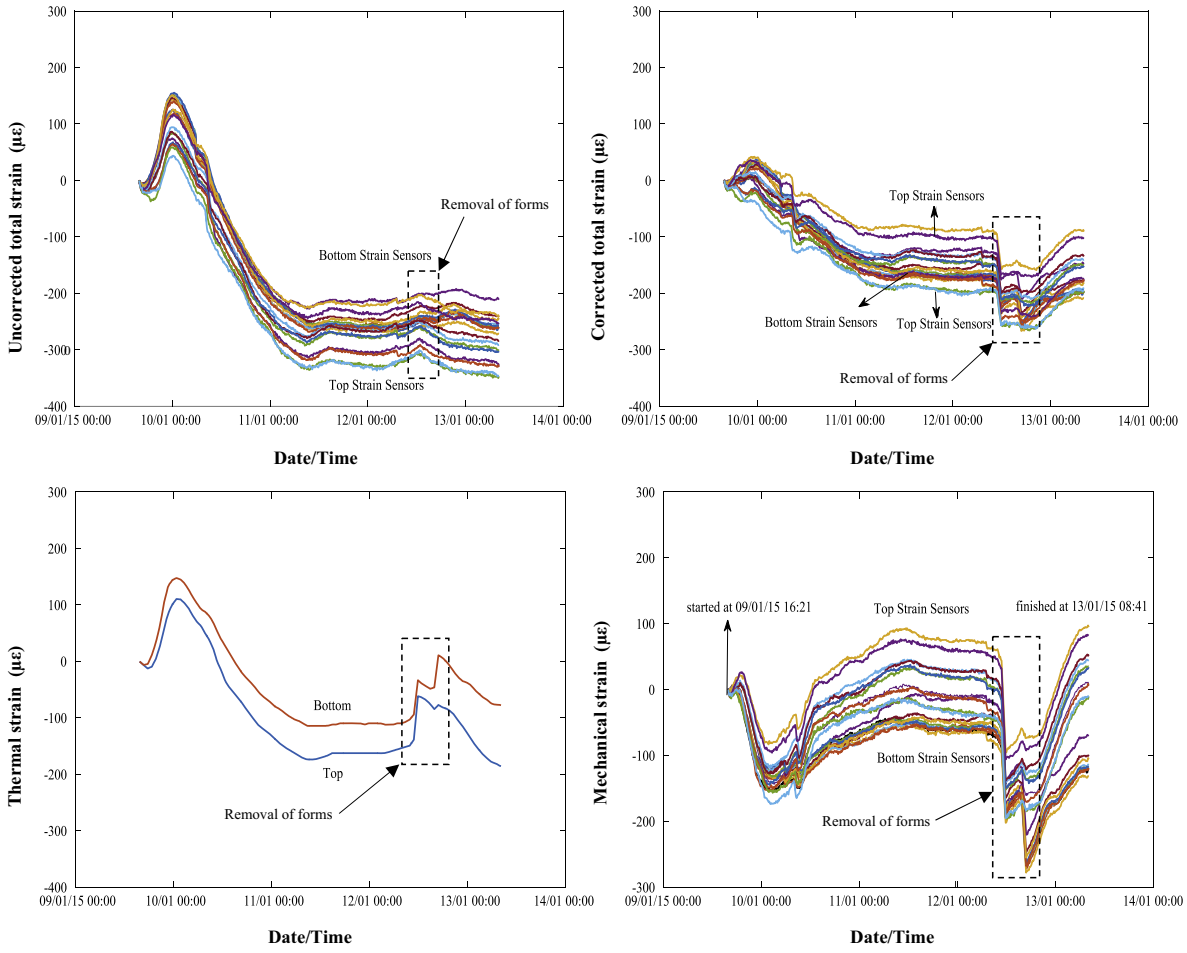

Fig. 5. Recorded mechanical strains during curing of BM1 (baseline = one hour post-casting).

(top mainly in tension and bottom in compression) occurs up to the same maximum top fibre strain of 100 με and a maximum bottom strain of 120 με. Therefore, by the end of the recorded curing period of BM1, a significant difference between top and bottom strains existed within the beam which translated to a net curvature and moment. These locked-in strains play a critical role when evaluating the change in strain due to transfer of prestress in the beams.

The differences observed in the strains developed during the curing (prior to transfer of prestress) of the TY7 and TYE7 beams illustrates the significant variability that can be present in outdoor concrete casting operations even with concretes that have the same mixture design.

5.1.2. Detensioning process

The entire detensioning process was captured for beams BM2, 3, 1 and 9 using the installed FBG sensors as they were able to acquire data up to 1000 Hz. Results of the detensioning process for BM2 and BM1 in the form of the mechanical strain variation with time are presented in Figs. 6 and 7, respectively. Note that the baseline for these strain readings was taken as the mechanical strain prior to detensioning.

In both the TY7 and TYE7 beams, a distinct difference in the strains developed along the top and bottom strands is evident. The bottom of the beams experience larger compressive strains as compared to the tops of the beams. This difference in top and bottom strains creates a curvature within the beam causing an upwards (negative) deflection or camber which is characteristic

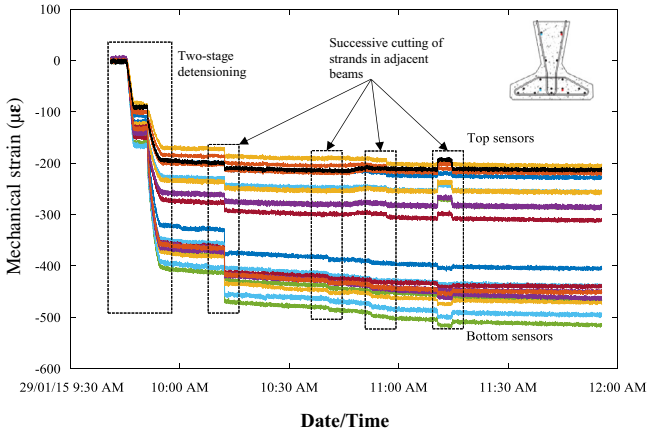

Fig. 6. Change in mechanical strain measured with FBG sensors in BM2 (TY7 internal beam) during the detensioning process (baseline = pre-detensioning).

of prestressed concrete girder design. Along the length of the beams, the top and bottom strain ranges vary between 100 με and 110 με for the TY7 beams, respectively and between 95 με and 105 με for the TYE7 beams, respectively. Part of this variation (approximately 20 με) may be attributed to variations in self-weight however, the remaining variation is likely the result of the restraint caused by the friction between the underside of the beam and the casting bed. Therefore, when comparing beams during various monitoring stages and when calculating losses due to

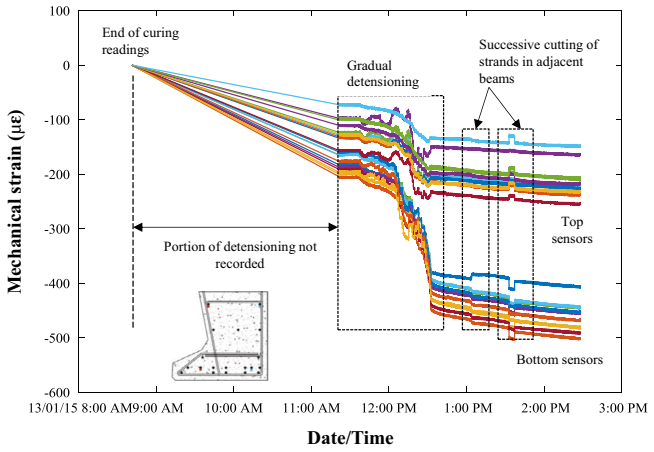

Fig. 7. Change in mechanical strain measured with FBG sensors in BM1 (TYE7 edge beam) during the detensioning process (baseline = pre-detensioning).

prestress, the average top and bottom strains along the lengths of the beams were assumed.

It is also evident that the TY7 beam experiences a slightly larger compressive strain change in the top of the beam (average top strain = −243 με) compared to the TYE7 beam (average top strain = −225 με). This is likely due to the differences in prestressing force, concrete compressive strength at the time of detensioning, and the section shape and geometry.

Results from the sensor data revealed that the detensioning procedures for the internal TY7 (BM2) and external TYE7 (BM1) beams were markedly different. A two-stage detensioning process was used for BM2 whereby the live end of the jacking head was detensioned first followed by release of the clamps near the dead end of the prestressing bed. Residual strains were then introduced into the beam during the cutting of the prestressing strands in adjacent beams along the prestressing bed.

During monitoring of the TYE7 beams, there was an approximate three hour gap between the end of beam curing data acquisition and the start of data acquisition for the detensioning process (refer to Fig. 7). Within this three hour period, the internal thermocouples installed within the beams registered a temperature change of +1.1 °C (thermal strain of 11 με) and the strain sensors registered negative strain changes of 200 με. This difference in strain is the result of the premature detensioning process carried out by the pre-casting facility operators before data acquisition could be re-started. The TYE7 beam (BM1) underwent a multi-staged and gradual detensioning process. According to the pre-casting facility operators, this multi-stage process was necessary as there was significantly higher tensile stress on the prestressing bed compared to the TY7 beams. As shown in Fig. 7, during the start of the detensioning process, the top section of BM1 undergoes a recoverable jump (reduction in compression) while the bottom of the beam undergoes a jump in net compression. It is theorized that this resulted from the friction between the underside of the beam and the casting bed that was induced by the detensioning process. Residual strains measured in BM1 were also introduced and recovered during the strand cutting process. After the cutting process, the top and bottom strains in both beams BM1 (TY7) and BM9 (TYE7) gradually decreased which represents the combined effects of early age creep and shrinkage.

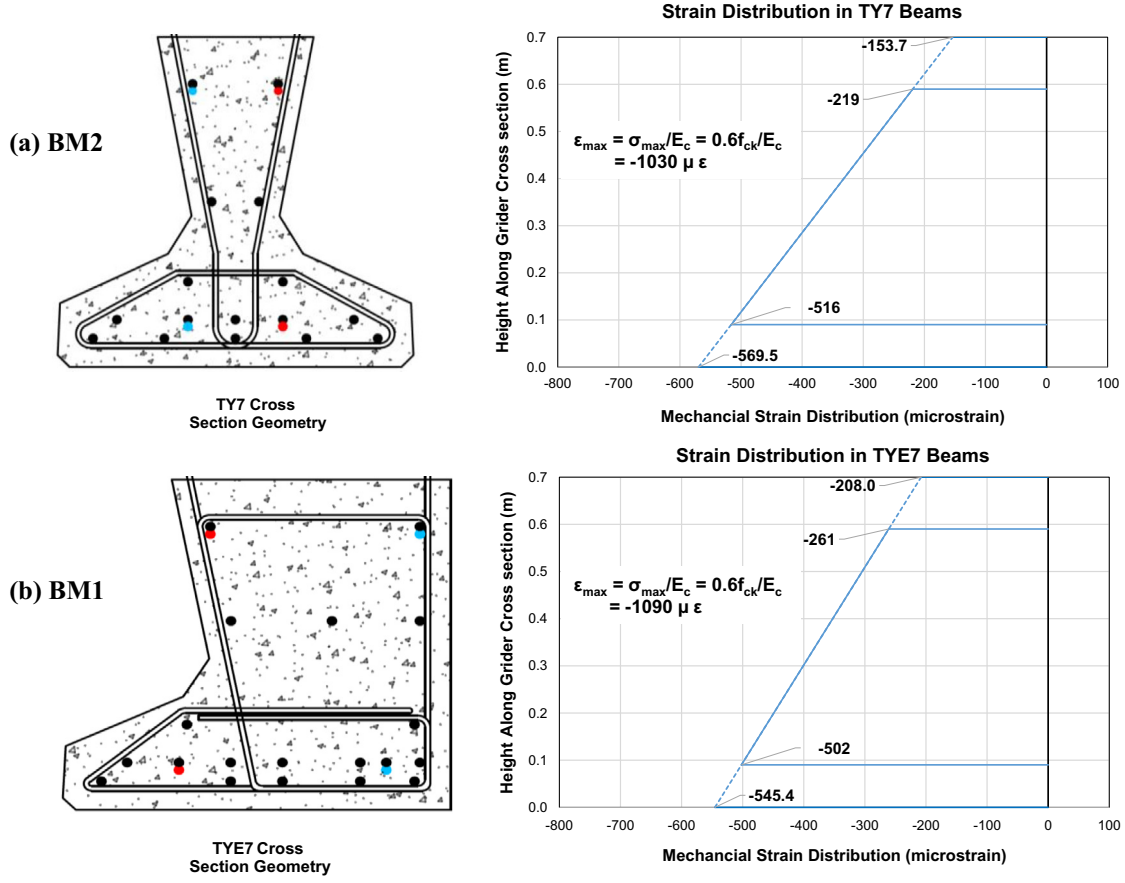

Fig. 8. Measured stress distribution at the time of prestress transfer for (a) BM2 and (b) BM1.

Based on the data captured during the detensioning process (Figs. 6 and 7), the maximum strains along the top and bottom can be compared with design limits. According to Eurocode 2, the maximum concrete compressive stress due to transfer of prestress is 0.6 f_{ck} where f_{ck} is the compressive strength of the concrete at the time of prestress transfer [1]. Using this limit on stress, a limit on strain can be computed by dividing the limiting stress by the concrete modulus of elasticity, E_c at the time of detensioning. Fig. 8 displays the measured and interpolated strain distribution for both BM2 and BM1 and presents the calculated maximum compressive strain limits as per Eurocode 2. Based on the measured strains, it is evident that they are well below (55% and 50% for BM2 and BM1, respectively) the compressive stress limits for both BM2 and BM1.

5.2. Beam storage, transport and installation

Following the detensioning process, the beams were transported to an outdoor temporary storage area within the prestressing yard prior to being transported to the bridge site. The beams were cast in January 2015 and were not transported to site until July 2015 and therefore, continued to undergo strain changes due to concrete shrinkage, creep and steel relaxation. In addition, the TYE7 beams (BM1 and BM9) received a second stage casting whereby part of the finished bridge deck slab was cast 55 days after casting. This slab induced additional flexural strains due to its own self-weight but also affected the amount of creep within the beam and would impose differential shrinkage strains between the newer slab concrete and the older concrete in the beam.

The entire strain history (from just before detensioning) of each beam is presented in Figs. 9–12 as spatial plots that show the distributed strains along the beams. Note that the values presented reference the baseline strain as the strain recorded at the time just prior to detensioning. Recall that 10 FBG (discrete) sensors were installed along both the top and bottom of each beam with a companion set of BOTDR (distributed) sensing cables.

Based on the results presented in Figs. 9 and 10, the distributed strain profile for the TY7 beams (BM2 and BM3) appears to be fairly uniform across their length. Both TY7 beams (BM2 and BM3) exhibited fairly similar strain changes within their first six months following casting. Based on the FBG readings, the largest change in strains occurred within the first 3 months following detensioning (average 337 με on top and 627 με on bottom) whereas the smallest strain change occurred between approximately 3 and 6 months just before bridge deck casting (average 93 με on top and 53 με on bottom). Based on these results it appears that a large portion of the creep and shrinkage occurred within the beams within approximately the first three months after casting. Note that BOTDR readings were only recorded up until 3 months (82 days) after casting. In general, the BOTDR strain values are slightly lower (less negative) than the FBG strain values. The top BOTDR strain values were particularly different than the top FBG strain values for both beams at the 3 month readings (75 days post-detensioning).

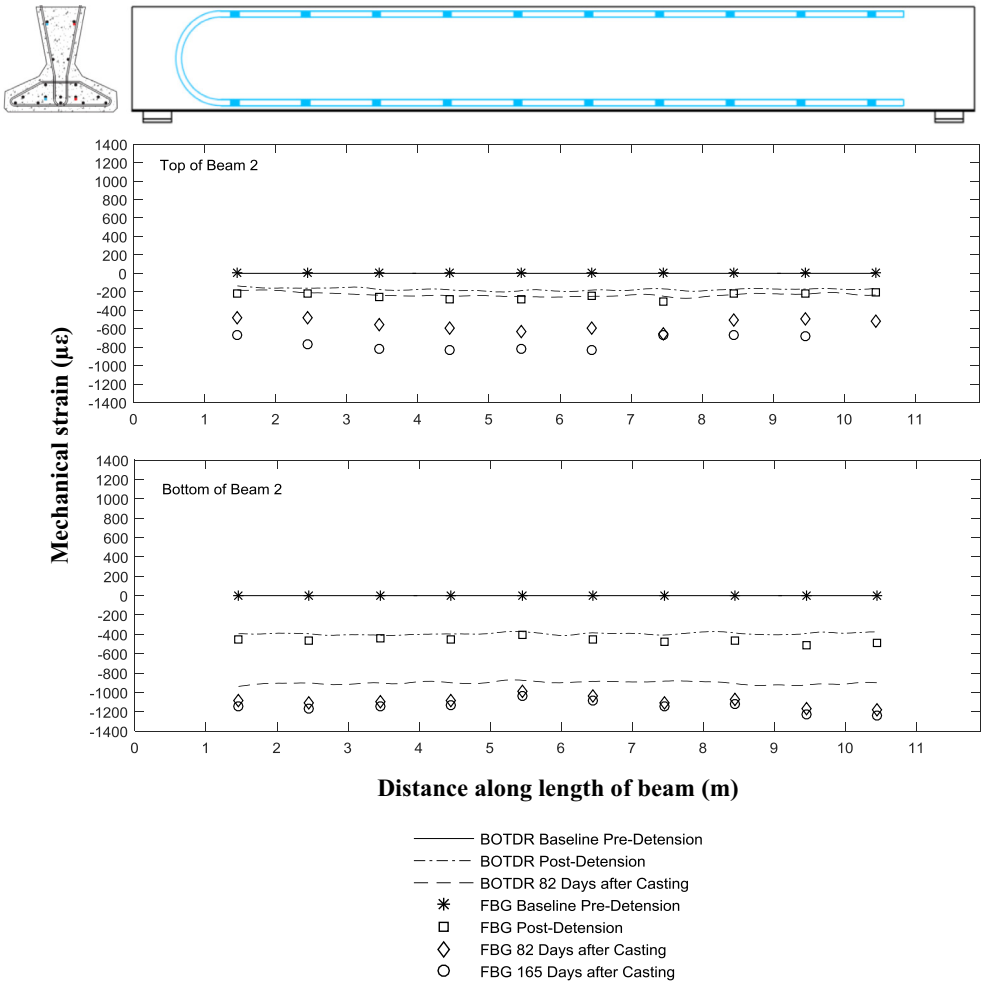

Fig. 9. Evolution of the distributed (BOTDR and FBG sensors) strain profile for BM2 (baseline = pre-detensioning).

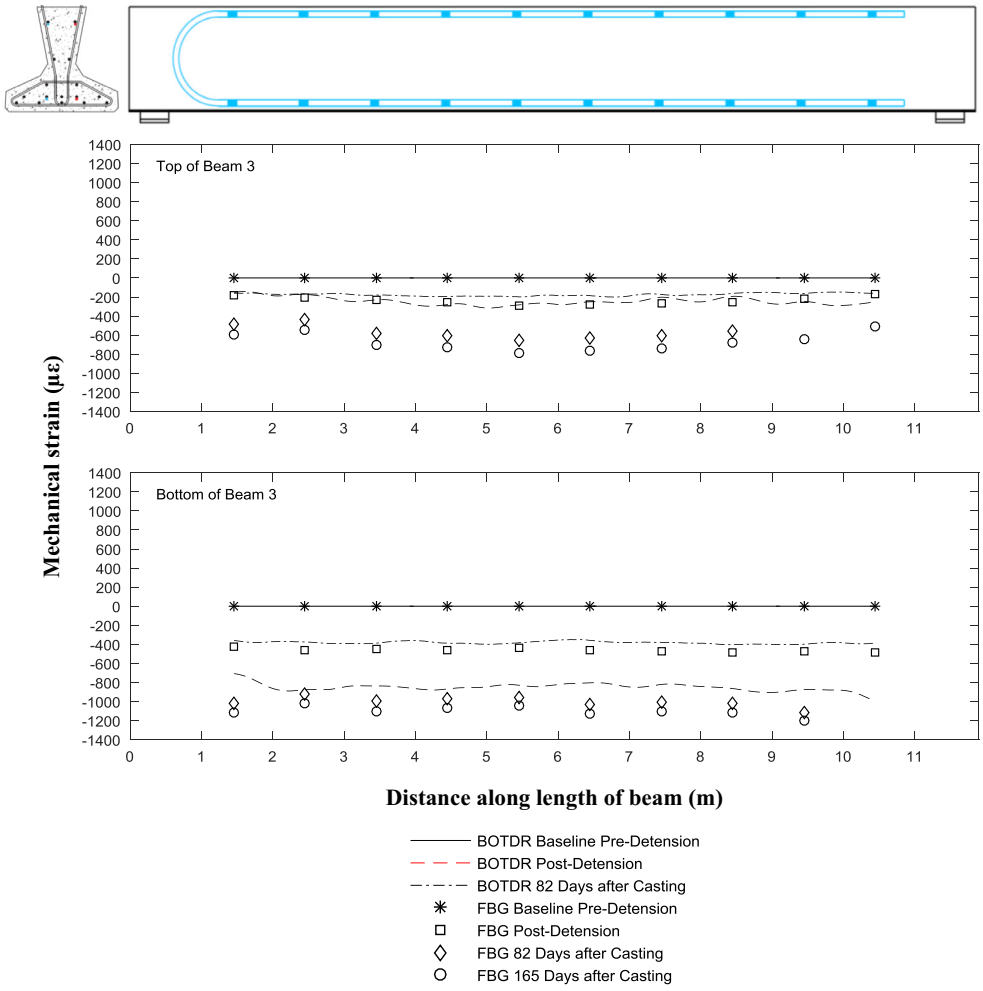

Fig. 10. Evolution of the distributed (BOTDR and FBG sensors) strain profile for BM3 (baseline = pre-detensioning).

Based on the results presented in Figs. 11 and 12 , the distributed strain profile for the TYE7 beams also appears to be fairly uniform across their length. Note that BOTDR readings are only available at pre-detensioning and at 95 days after casting. Similar to the TY7 beams, BM1 and BM9 both experienced the largest strain changes between post-detensioning and 3 months following casting (average 416 με on top and 615 με on bottom) whereas the smallest strain change occurred between approximately 3 and 6 months just before bridge deck casting (average 28 με on top and 14 με on bottom). Similar to the TY7 beams these results indicate that the majority of the early age creep and shrinkage experienced by the TYE7 beams occurred within the first 3 months after casting. In both BM1 and BM9, the top and bottom BOTDR strain readings appear to be in good agreement with the FBG strain readings.

In general, from the time just before pre-detensioning (after initial concrete curing) the TY7 beams experienced a larger strain change (30% on top and 18% on bottom) compared to the TYE7 beams in their first 6 months after casting.

6. Early-age prestress loss estimation

6.1. Prestress loss predictions

Total prestress losses are divided into two components: instantaneous losses and time-dependent losses. Instantaneous losses for prestressed concrete include the relaxation of steel prior to detensioning, losses associated with shrinkage of concrete, and the losses due to elastic shortening of the concrete at the time of prestress transfer. The time-dependent losses include long-term losses due to relaxation of steel, shrinkage and creep. Formulae provided in Eurocode 2 [1] have been used as the basis for calculating the predicted prestress losses. Losses due to steel relaxation, elastic shortening of concrete, shrinkage and creep were all considered. Several stages of construction, as summarised in Table 1, were evaluated and the prestress losses at each stage were estimated using the Eurocode 2 (EC2) provisions. These were then compared with the prestress losses back-calculated from the measured fibre optic strain data, which are presented in Section 6.2.

6.1.1. Tendon relaxation

Relaxation of the tendons, due to the loss of tension over time for a fixed length and temperature, is a property of the steel and a function of the ratio between the initial prestressing force and the tensile strength. Relaxation progresses more rapidly than either concrete shrinkage or creep [18]. Using Eurocode 2, the time-dependent change in tendon stress can be calculated using Eq. (4),

$$\Delta\sigma_{p,REL,i} = 6.6(\sigma_{pi})\rho_{1000}e^{9.1\mu}\left(\frac{t}{1000}\right)^{0.75(1-\mu)} \times 10^{-6} \quad (4)$$

where $\Delta\sigma_{p,REL,i}$ is the change in prestress due to steel relaxation at time t (in hours), σ_{pi} is the initial level of prestress and ρ_{1000}

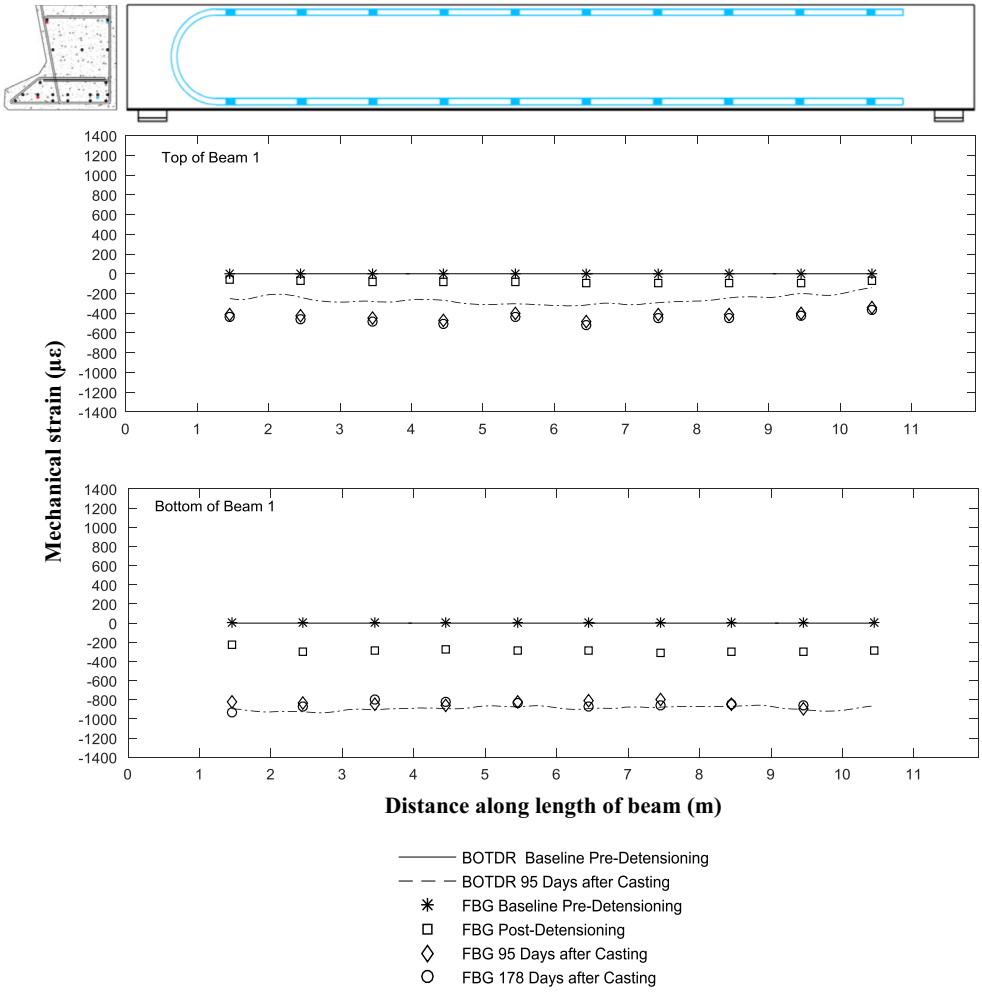

Fig. 11. Evolution of the distributed (BOTDR and FBG sensors) strain profile for BM1 (baseline = pre-detensioning).

depends on the prestressing class (in this case is equal to 2.5%) and μ is given by

$$\mu = \frac{\sigma_{pi}}{\sigma_{pk}} \tag{5}$$

where σ_{pk} is the characteristic strength of the prestressing strand. The change in prestressing force, $\Delta P_{REL,i}$ is then calculated as

$$\Delta P_{REL,i} = \Delta\sigma_{p,REL} A_p \tag{6}$$

This formula is used to calculate the prestress loss due to steel relaxation prior to detensioning of the tendons. Longer term relaxation will be taken into account by also considering the interactive effects of shrinkage and creep as is discussed in the upcoming sections.

6.1.2. Elastic shortening of concrete

After the concrete has reached adequate compressive strength, usually between 80 and 90% of f_{ck}, the prestressing strands are detensioned at the jacking head and the prestress is transferred as a compressive force into the concrete. Both the concrete and the bonded tendons shorten due to the applied compressive force, thereby reducing the prestressing tension in the tendons. In cases where the tendon arrangements is such that the centroid of the prestressing steel and the centroid of the concrete section are not concurrent, an eccentricity, e, exists which causes an additional moment equal to the product of the total prestressing force and the eccentricity. This moment creates bending stresses in the section and generates curvature in the beam resulting in an upward (negative) deflection or camber. Eq. (7) allows for the calculation of the associated change in prestress in the tendons due to elastic shortening of concrete.

$$\Delta P_{EL}(t) = \frac{A_p \frac{E_p}{E_{cm}(t)} \sigma_c}{1 + \frac{E_p}{E_{cm}(t)} \frac{A_p}{A_c}\left(1 + \frac{A_c}{I_c} e^2\right)} \tag{7}$$

$$\sigma_C = \frac{P}{A_c} + \frac{(Pe)e}{I_c} \tag{8}$$

where

A_p = area of all the prestressing strands at a particular cross-section along the beam
E_p = modulus of elasticity of the prestressing steel = 195 000 MPa
$E_{cm}(t)$ = modulus of elasticity of the concrete at the time of detensioning
A_c = area of the concrete section
I_c = moment of inertia of the concrete section about its centroid
P = total prestressing force (sum of all tendons)
e = tendon eccentricity (distance between centroid of the concrete section and the centroid of the tendons).

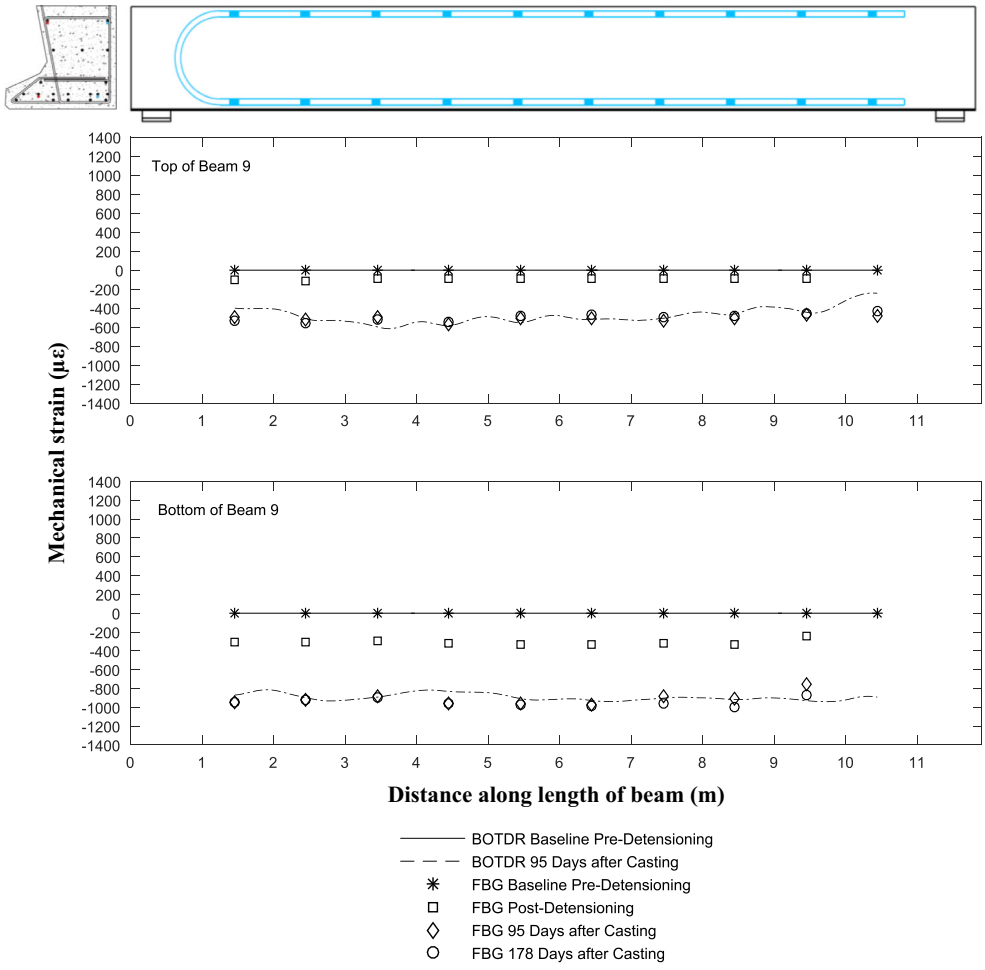

Fig. 12. Evolution of the distributed (BOTDR and FBG sensors) strain profile for BM9 (baseline = pre-detensioning).

Table 3
Calculated prestress losses according to Eurocode 2 based on concrete material properties.

Event	TY7		TYE7	
	$\Delta\sigma$ [MPa]	$\Delta\sigma/\sigma_{pi} \times 100\%$	$\Delta\sigma$ [MPa]	$\Delta\sigma/\sigma_{pi} \times 100\%$
Tendon relaxation	15.0	1.1%	13.5	1.0%
Transfer of prestress*	72.6	5.2%	68.5	4.9%
Total instantaneous losses	87.6	6.3%	82.0	5.9%
82 days (TY7) and 95 days (TYE7) after casting†	171.0	12.3%	154.8	11.1%‡
165 days (TY7) and 178 days (TYE7) days after casting (before deck casting)†	189.6	13.6%	167.9	12.1%
Final long term losses (120 years)	274.5	19.7%	266.5	19.1%

Note: recall that σ_{pi} = 1393.3 MPa.
* Calculation accounts for tendon relaxation losses prior to detensioning.
† Includes all instantaneous losses (i.e. cumulative losses) and creep losses were calculated based on the reduced prestressing forces after initial prestress losses.
‡ Includes additional effect of first slab casting (additional flexural strain due to dead load only).

6.1.3. Combined calculation of time-dependent losses

Time-dependent losses are often calculated in a combined form to account for the interaction between creep, relaxation and shrinkage as presented in Eq. (9). The original formulation was proposed by Neville et al. [19] and has since been adopted in various design procedures and codes for prestressed concrete such as Eurocode 2.

$$\Delta P(t)_{C+S+R} = A_p \Delta\sigma_{p,c+s+r} = A_p \frac{\varepsilon_{cs} E_p + 0.8\Delta\sigma_{p,REL} + \frac{E_p}{E_{cm}}\varphi(t,t_0)\sigma_{c,qp}}{1 + \frac{E_p}{E_{cm}}\frac{A_p}{A_c}(1 + \frac{A_c}{I_c}e_{cp}^2)[1 + 0.8\varphi(t,t_0)]} \quad (9)$$

Where,

A_p = area of all the prestressing strands at a location x along the beam
ΔP_{C+S+R} = absolute value of the variation of force of the in the tendons due to creep, shrinkage and relaxation at location x, at time t (days)
ε_{cs} = estimated shrinkage strain at time t (days)
E_p = modulus of elasticity for the prestressing steel
E_{cm} = modulus of elasticity for the concrete at 28 days
$\Delta\sigma_{p,REL}$ = absolute value of the variation in stress in the tendons at time t, due to the relaxation of the prestressing steel.

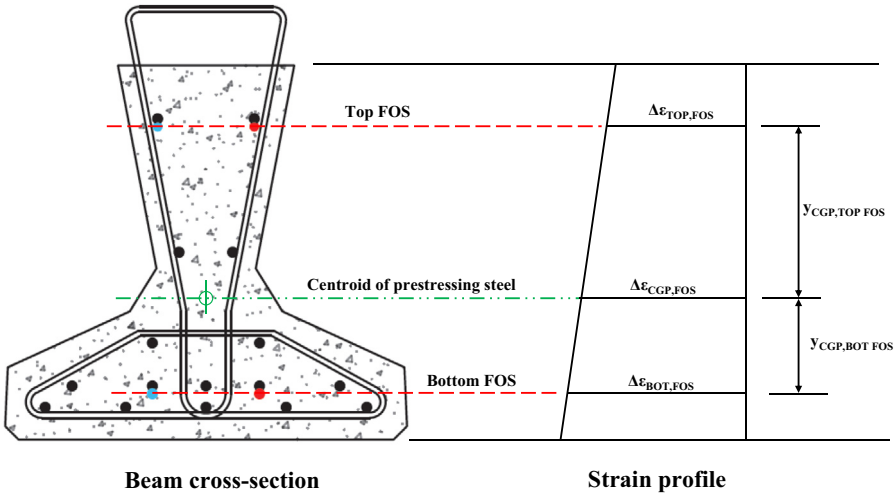

Fig. 13. Strain distribution based on fibre optic sensor locations.

$\varphi(t,t_0)$ = creep coefficient at time t (in days) for a load application occurring at time t_0.
$\sigma_{c,qp}$ = stress in the concrete adjacent to the tendons at time t, due to self-weight and initial prestress and other quasi-permanent actions.
A_c = area of the concrete section
I_c = moment of inertia of concrete section about its centroid
e_{cp} = tendon eccentricity (distance between centroid of the concrete section and the centroid of the tendons).

The 0.8 term is an ageing coefficient intended to account for the reduction in both relaxation and creep due to the interaction of shrinkage, creep and relaxation effects. In calculating the long term losses, the reduced prestressing force that accounts for the initial prestress losses during curing and detensioning was used. The total losses due to all instantaneous and time-dependent effects can then calculated using Eq. (10) and the percent loss is calculated based on the initial prestress force as in Eq. (11).

$$\Delta P_{TOT} = \Delta P_{EL,i} + \Delta P_{REL,i} + \Delta P_{C+S+R} \tag{10}$$

$$\text{prestress loss} = \frac{\Delta\sigma_{cgp}}{\sigma_{pi}} = \frac{\Delta\varepsilon_{cgp}E_p}{\sigma_{pi}} \times 100\% \tag{11}$$

6.1.4. Total calculated prestress losses

Using the equations presented in the previous sections, the total prestress losses for both the TY7 (BM2 and BM3) and TYE7 (BM1 and BM9) beams can be calculated. However, a variety of different parameters and variables must be estimated and/or calculated based on the real beam properties, the associated time frames, and any relevant environmental factors. The time of transfer of the prestressing force was based on the actual detensioning dates. Detensioning occurred 7 days after casting for the TY7 beams and 4 days after casting for the TYE7 beams. Prior to detensioning, both sets of beams were left to cure in ambient (outdoor) conditions without supplemental heat or moisture. The targeted design strength at the time of detensioning was 50 MPa. As discussed in Section 5.1, due to lower ambient temperatures and unfavourable weather conditions, the TY7 beams took longer than anticipated to reach the target strength (7 days). Based on the Eurocode 2 predicted equations and estimated materials properties, instantaneous and time dependent losses were calculated at the corresponding stages when sensor measurements were taken (refer to Table 1) and are summarised in Table 3.

Based on the calculated values it appears that the TY7 beams will experience slightly higher prestressing losses over their lifespan (approximately 120 years or 43,800 days) as compared to the TYE7 beams. Approximately 70% and 65% of the total losses are predicted to occur prior to casting of the concrete deck for the TY7 and TYE7 beams, respectively.

6.2. Prestress loss estimation based on fibre optic sensor data analysis

Both fibre optic sensor systems, FBGs and BOTDR, measured strain change values for the TY7 and TYE7 beams at the various construction stages. In order to calculate the prestress losses based

Table 4
Measured cumulative prestressed losses based on FBG measured strains compared with EC2 predicted losses.

Event	TY7 Beams			TYE7 Beams		
	BM2 ($\Delta\sigma$, MPa)	BM3 ($\Delta\sigma$, MPa)	EC2 ($\Delta\sigma$, MPa)	BM1 ($\Delta\sigma$, MPa)	BM9 ($\Delta\sigma$, MPa)	EC2 ($\Delta\sigma$, MPa)
Pre-detensioning/curing	0.9% *(12.4)*	†0.9% *(12.4)*	1.1% *(15.0)*	††0%	††0 %	1.0% *(13.5)*
Transfer of prestress	6.8% *(95.3)*	6.7% *(94.0)*	6.3% *(87.6)*	5.6% *(77.4)*	6.1% *(84.4)*	5.9% *(82.0)*
82 days (TY7) and 95 days (TYE7) after casting	14.8% *(206.4)*	13.7% *(190.6)*	12.3% *(171.0)*	13.2% *(183.3)*	13.7% *(191.3)*	11.1% *(154.8)*
165 days (TY7) and 178 days (TYE7) after casting	15.8% *(221.1)*	15.0% *(209.0)*	13.6% *(189.6)*	13.4% *(186.1)*	14.0% *(194.7)*	12.1% *(167.9)*
Final long term losses (120 years)	n/a	n/a	19.7% *(274.5)*	n/a	n/a	19.1% *(266.5)*
Measured 6 month losses/EC2 Predicted Final Prestress Loss	0.9% *(12.4)*	†0.9% *(12.4)*	1.1% *(15.0)*	††0%	††0 %	1.0% *(13.5)*

† Baseline data at one hour post-casting was unavailable for BM3, therefore, it was assumed that BM3 experienced similar pre-detensioning losses as BM2 as they were cast next to each other at the same time. Measurements for BM3 were available at all other stages of monitoring.

†† Note that an overall positive average change in strain was measured during the curing of the TYE7 beams. Therefore, since prestress cannot be added, it was assumed that no net loss had occurred during this period. Refer to Section 5.1.1 for further explanation. It was assumed that BM1 and BM9 behaved similarly prior to transfer of prestress as they were cast next to each other at the same time.

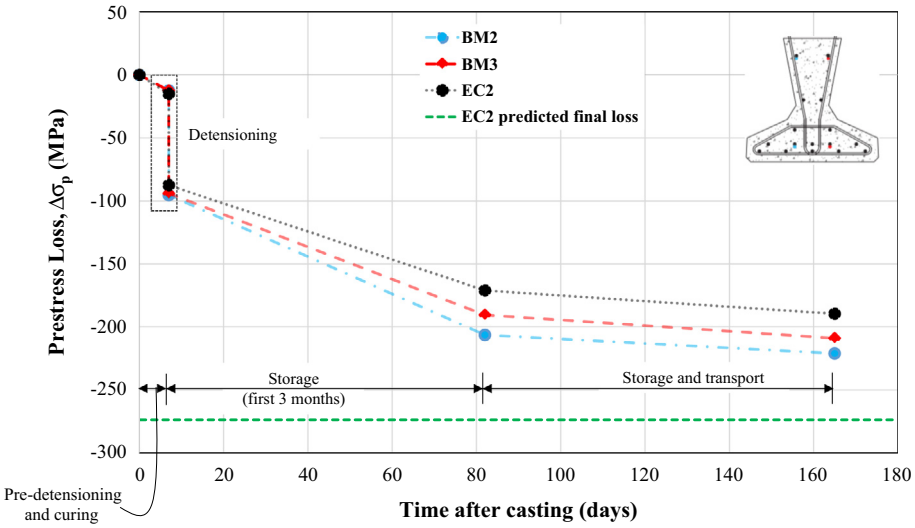

Fig. 14. Evolution of prestress losses with time for the TY7 beams (BM2 and BM3).

on the strain changes measured in the top and bottom sensor arrays, the strain values had to be interpolated to calculate the strain at the centroid of the prestressing steel tendons, ε_{cgp}. The change in prestress was then calculated using Eq. (11). Fig. 13 illustrates the measured strain distribution of a TY7 beam section. Given that both the FBG and BOTDR sensors provided measured strains along the length of the beam (at the top and bottom of the section), the average value along the length of the cable was used to calculate the prestress losses.

Based on the uniform spatial strain distributions observed in Figs. 9–12, using the average strain to estimate the prestress losses appears to be valid. The primary assumption in these calculations is that there is perfect bond between the concrete and the prestressing strands. In this way, it is assumed that the FBGs that are attached to the underside of the prestressing strands but mainly surrounded by concrete, are subjected to the same strain as that experienced by the prestressing strands. Prior to detensioning it is typically assumed that anchorage set and relaxation of the prestressing strands occurs and accounts for the initial prestress losses. Note that because of the detensioning procedures adopted, losses due to anchorage setting were assumed to be negligible. As the internal TY7 and TYE7 beams were detensioned seven and four days after casting, respectively, and no supplemental curing or heating was provided, it has been assumed that significant drying shrinkage occurred prior to transfer of prestress.

Table 4 presents the EC2 predicted losses and the calculated prestress losses based on the measured strain data from the FBG sensors for the internal TY7 beams and the TYE7 edge beams.

Figs. 14 and 15 present the graphical representation of Table 4 and the evolution of prestress losses for all four beams as compared with EC2 predicted values. Note that pre-detensioning strain data was not available for BM3 and BM9 and so these strain changes have been assumed to be similar to those experienced by BM2 and BM1, respectively. This is a valid assumption as the TY7 beams (BM2 and BM3) were cast adjacent each other on the same pre-casting bed, with the same concrete mixture and at the same time; likewise for the TYE7 beams. All loss percentages have assumed an initial total tendon stress, σ_{pi} of 1393 MPa/strand ($0.75f_{pu}$) based on the initial design parameters for the prestressed beams and were confirmed by the prestressing yard operators.

Given that the individual effects of creep, shrinkage and steel relaxation have been measured as a lump sum, the total time-

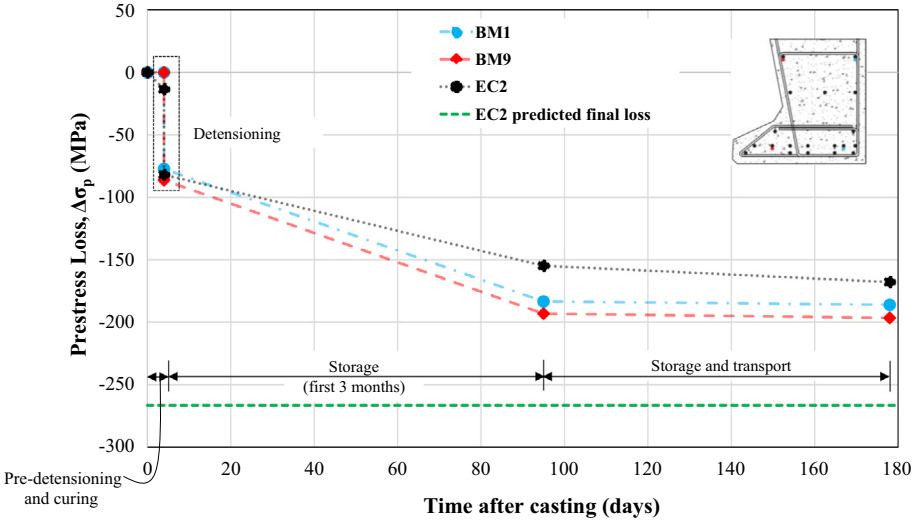

Fig. 15. Evolution of prestress losses with time for the TYE7 beams (BM1 and BM9).

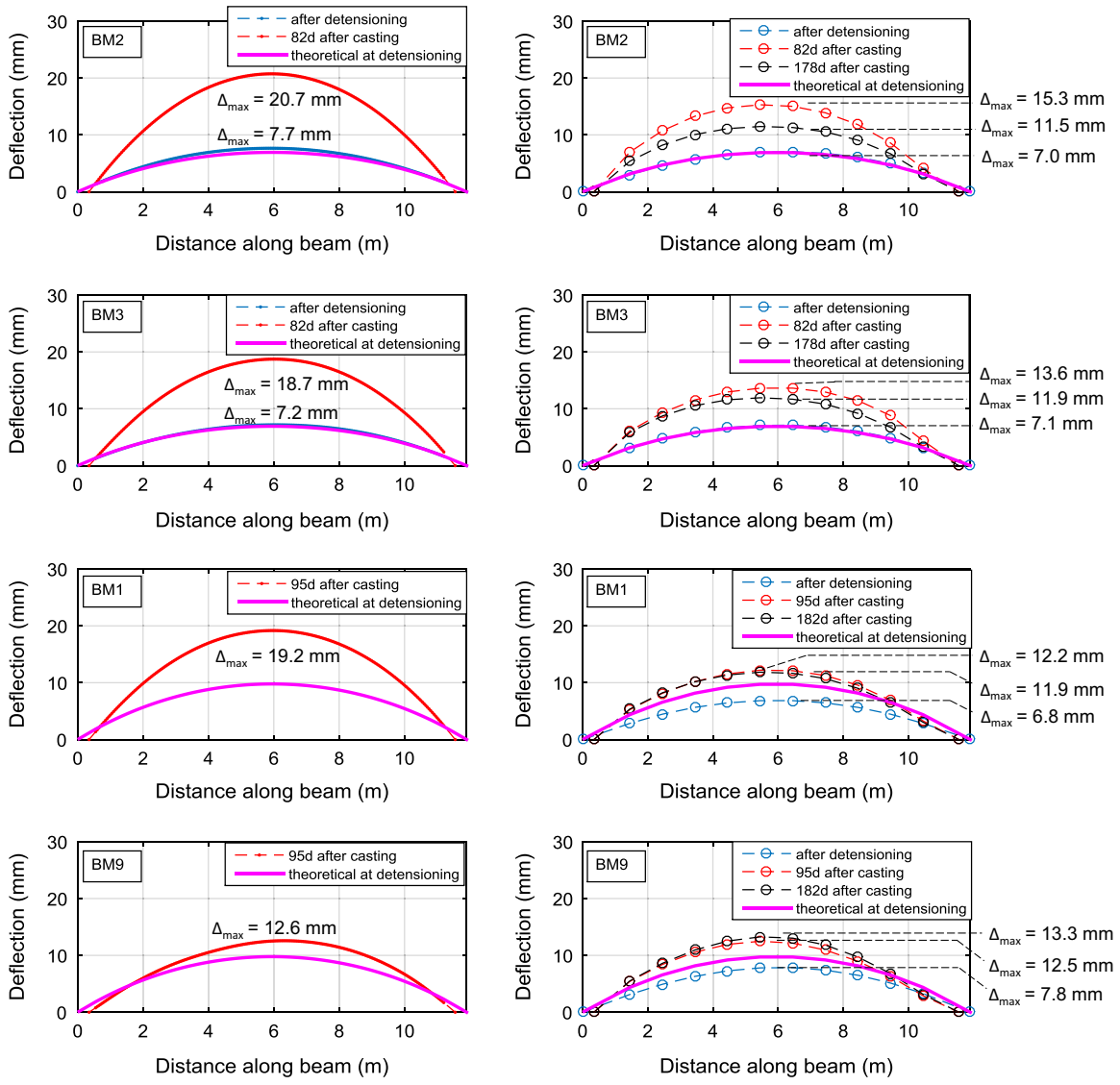

Fig. 16. Theoretical and estimated vertical camber measurements based on (a) BOTDR sensor data and (b) FBG sensor data.

dependent losses in the first 3 and 6 months following casting are reported. In general, the code-predicted prestress losses appear to underestimate the prestress losses calculated using the embedded fibre optic sensors. However, the code-based equations were derived primarily for predicting ultimate prestress losses and therefore, may not be suitable for calculating early-age prestress losses within the first six months after beam casting. It is important to note that the loss of prestress with time is a non-linear process, and therefore, is represented in Figs. 14 and 15 as dashed lines in order to present the general decreasing trend of the theoretical and measured prestress losses. Based on the calculated results, the TY7 beams experienced 11% higher prestress losses after 6 months as compared with the TYE7 beams. This difference seems to stem from additional losses due to early age shrinkage and elastic shortening. The additional loss due to shrinkage is a result of the manufacturing conditions as the curing period for the TY7 beams was 3 days longer than that of the TYE7 beams. Based on the measured strain data, an average of 79% and 72% of the prestress losses predicted to occur over the design life of the beams (using Eurocode 2 equations) have occurred within the first 6 months after casting for the TY7 and TYE7 beams, respectively. Within both sets of beams, the majority of the time dependent losses due to creep, shrinkage and relaxation were measured to occur within the first three months after casting (refer also to Section 5.2 for additional discussion). This is in good agreement with studies performed by Garber et al. [4] who concluded that the majority of prestress losses occurred within the first 4 months following casting. In the following three month period between storage and erection on the bridge abutments, the average measured losses and the EC2 predicted compared closely for the TY7 beams. In the same period, the EC2 predicted losses overestimate the average measured losses for the TYE7 beams (refer to Figs. 14 and 15). Based on these early age results, it may be inferred that, compared with the EC2 predicted total prestress losses, the long term losses may be slightly higher and slightly lower for the TY7 and TYE7 beams, respectively. However, the next phases of this research will be aimed at evaluating the prestress losses of the beams after bridge completion and in-service.

7. Estimation of camber based on fibre optic strain data

Using the measured strain values along the tops and bottom of the beams, the curvature and deflection along the length of the beam can be estimated using Bernoulli-Euler elastic beam theory. Using basic moment-curvature relationships, the measured top and bottom strain values can be used to back-calculate the camber in the beam.

$$\kappa(x) = \frac{M(x)}{EI} \tag{12}$$

Performing double integration of the curvature function will allow for the calculation of the deflection along the length of beam.

$$w(x) = \int\int \kappa(x)dxdx \tag{13}$$

Integration constants can be determined based on the following assumptions for a simply-supported beam:

$$\begin{aligned} w\prime(x = l/2) &= 0 \\ w(x = 0 = l) &= 0 \end{aligned} \tag{14}$$

In this study, numerical integration based on the trapezoidal rule was performed to evaluate Eq. (13). Curvature values along the length of the beam (corresponding to sensor locations) can be calculated using the following relationship:

$$\Delta\kappa(x) = \frac{\Delta\varepsilon_{bot}(x) - \Delta\varepsilon_{top}(x)}{d} \tag{15}$$

The change in strain values correspond to the difference in strains measured before and after some event (e.g. the detensioning process). Therefore, the associated curvature represents the curvature due to the particular event. In this study, the vertical camber was calculated at several stages: immediately following detensioning, after approximately 3 months following casting, and after beam erection but prior to casting of the concrete deck. Note that the value of 'd' in Eq. (15) is the vertical distance between top and bottom sensor locations. Both BOTDR and FBG sensor data was used to calculate camber for all beams however, due to equipment errors on the day of detensioning, BOTDR data was not available for the detensioning of the TYE7 beams (BM1 and BM2) and just prior to deck casting. Based on design calculations and assumptions, the estimated pre-cambers (following the transfer of prestress) can be computed using Eqs. ((16–18)).

$$w(x)_{tot} = w_{SW} + w_{PE} \tag{16}$$

$$w(x)_{SW} = \frac{qx}{24E_cI_g}(l^3 - 2lx^2 + x^3) \tag{17}$$

$$w_p(x) = \frac{Pex}{2E_cI_g}(l - x) \tag{18}$$

Where,

$w(x)_{tot}$ = total deflection (camber) of beam at transfer of prestress
$w(x)_{SW}$ = deflection of beam at transfer due to self-weight
$w(x)_p$ = deflection (camber) of beam at transfer due to prestressing force
q = self-weight of girder per unit length
P = total prestressing force at the time of transfer (based on EC2 calculations in Section 6)
e = tendon eccentricity
E_c = modulus of elasticity of concrete at the time of transfer (refer to Table 2)
I_g = gross moment of inertia of concrete section
l = length of beam = 11.9 m.

The maximum midspan cambers due to the transfer of prestress were 7 mm and 10 mm for the TY7 and TYE7 beams, respectively. However, no measurements were taken of the actual cambers following detensioning. Fig. 16 presents the back-calculated vertical cambers for all four beams. Note that the span length used to calculate the camber following detensioning was 11.9 m as the beams rested at their extreme most ends. During storage and at beam erection, the beams rested on wooden blocks and bearings, respectively that were spaced at 11.2 m. This difference in span length has been accounted for in the camber estimates. In addition, the theoretically calculated cambers at the time of prestress transfer (detensioning) according to Eq. (16) have been plotted alongside the FOS-estimated values.

Based on the estimated camber data, it appears that the BOTDR and FBG data provide very similar estimates of the pre-camber for the TY7 beams even though there were fewer integration points available in the FBG data set. In addition, both fibre optic sensor systems were able to calculate pre-camber values (immediately after the transfer of prestress) for the TY7 beams that were in very close agreement (within 9%) with those predicted during the design. In the case of the TYE7 beams, the theoretical camber overestimated the camber estimated by the fibre optic sensors by up to 32%.

It is evident that beam cambers increase significantly within the first three months following casting and up until erection. Relative to the camber values measured immediately after detensioning, the final camber (at the time of erection) were, on average 1.7 and 1.2 times higher for the TY7 and TYE7 beams, respectively. This effect has been reported by several other researchers and is primarily the result of the changing creep effects within the concrete [20–23]. In general, the FBG measured results seem to be fairly consistent within all beams and time stages measured. However, the BOTDR results for the estimated camber for BM2, BM3 and BM1 at approximately 3 months following casting are up to 35% larger compared with the corresponding FBG sensor estimated cambers. This difference results from the difference in recorded strains presented in Section 5.2. In beams BM2, BM3 and BM1 the measured top BOTDR strain values in particular lagged behind the FBG strain values. Also of interest is the change in camber values between the estimated values at 3 months and values at 6 months after casting. It would be expected that the camber values of the individual beams would increase over time due to concrete creep which was observed in the TYE7 beams in which their camber values increased slightly (or changed negligibly). However, the TY7 beams' camber values at 6 months decreased compared with their three month values. Recall that in Table 1, strain readings were recorded after the beams had been installed on the bridge bearings but also after the reinforcing steel for the concrete deck was installed. The deck reinforcing was primarily supported by the internal TY7 beams and caused a sagging moment in the beams and thereby reduced the FOS-estimated cambers.

Overall, using the measured strain values obtained from the fibre optic sensor systems (in particular those measured with the FBG sensors) provide a promising method for estimating in-service deflections of prestressed concrete bridge beams.

8. Conclusions

This study evaluated the early-age behaviour of four full-scale prestressed concrete bridge beams utilising the combined technologies of distributed (BOTDR) and discrete (FBG) fibre optic sensors. The entire curing and detensioning process of the beams were captured in great detail along their length. Additional monitoring data captured the strain evolution of the beams from just

after they were detensioned up until they were lifted onto the bridge abutments. Based on the analysis of the results, several important findings have arisen from this work.

1. Using both discrete (FBG) and distributed (BOTDR) fibre optic sensor technologies allowed for a relatively quick and robust installation with a reduced number of routing cables and connectors as compared to more conventional electrical-based sensing systems. Although the installed system has been able to capture the early age behaviour of the beams, evaluating the long term performance of such systems will require future monitoring work and research. However, due to their chemically inert nature, the fibre optic cables themselves could last as long as the structure itself with only the optical connectors and analysers requiring long term attention. Furthermore, the successful production of 'self-sensing' prestressed concrete beams is highly dependent on the coordinated efforts of the monitoring engineers, beam fabricators and structural designers prior to beam fabrication.
2. The interpretation of the strains developed in the concrete prior to detensioning is a highly complex process. Both the TY7 and TYE7 beams exhibited distinctly different strain loss characteristics in the first several days after casting. In particular, it was hypothesised that the restraint created by the beam formwork led to locked-in thermal strains that caused net tension in the top of the beam and net compression in the bottom of the beam. Overall, this effect counteracted the early-age concrete shrinkage strains and created insignificant prestress losses within the TYE7 beams prior to the transfer of prestress.
3. The FBG sensors were able to capture the detensioning processes for both TY7 and TYE7 beams in real time and in great detail. Due to the restraint on the soffit of the TYE7 beams provided by the prestressing bed, the top of the beam was temporarily placed in tension during the detensioning process. The TY7 beams experienced slightly higher average prestress losses due to elastic shortening as compared to the TYE7 beams (average of 5.9% versus average of 5.3%, respectively). The maximum compressive strains developed during the detensioning process were well within the compressive limits defined in Eurocode 2. Compared with the predicted values of prestress loss due to elastic shortening, the measured values were within 1% and 3% for the TY7 and TYE7 beams, respectively.
4. In both the TY7 and TYE7 beams, the majority of the time-dependent losses (creep, shrinkage and relaxation) occurred within the first three months after the beams were cast. Strains along the lengths of the beams were uniform along both the tops and bottoms of all beams during each stage of measurement.
5. In comparing the BOTDR and FBG sensor systems, the BOTDR strain readings compared fairly well to the FBG strain readings however, in some cases, the BOTDR strain readings provided higher strain values (less compression) than the FBG strain readings.
6. Measured prestress loss values for the TY7 and TYE7 beams approximately 6 months after casting were 79% and 72% of the ultimate prestress losses predicted by Eurocode 2, respectively.
7. The theoretically calculated cambers (at time of detensioning) were within 9% of the estimated cambers (based on fibre optic sensor data) for the TY7 beams. In the case of the TYE7 beams, the theoretically calculated cambers (at time of detensioning) overestimated the estimated cambers (based on fibre optic sensor data) by 32%. By estimating the cambers at various times up until the beam erection, they were found to increase significantly (between 1.2 and 1.7 times the estimated camber at detensioning). This preliminary study demonstrated the possibility of using the installed sensor system in combination with simple beam theory to measure deflections under service load conditions.

The primary aim of this research was to demonstrate that integrated sensing systems can become viable tools for monitoring strain evolution in concrete bridges and can be used to establish comprehensive baselines to inform long term bridge monitoring and asset management programmes. In addition, the lessons learned from this study can be applied on future projects and on more complex structures such as post-tensioned containment vessels, nuclear structures, and balanced cantilever bridge construction.

Acknowledgements

The authors gratefully acknowledge the EPSRC and Innovate UK for funding this research through the CSIC Innovation and Knowledge Centre (EPSRC grant reference number EP/L010917/1); the invaluable facilitation of the installation work from Liam Brunning of Explore Manufacturing and his team; the on-site assistance of Mahul Patel, Jason Shardelow, Peter Knott, Hyungjoon Seo of CSIC and Jules Birks of Mott-MacDonald (formerly of CSIC); the technical assistance in sensor development and procurement of Cedric Kechavarzi and Philip Keenan of CSIC; James Oliver, Matthew Timmis, Brad Stanaway and Phil Holland of Laing O'Rourke; and Ruth Platt and Mike Henwood of Atkins for providing their invaluable support for this project. Additional data related to this publication is available at the University of Cambridge data repository.

References

[1] EN 1992-1-1:2004 – Eurocode 2: Design of concrete structures – Part 1–1: General rules and rules for buildings. 2004.
[2] American Association of State Highway and Transportation Officials. AASHTO-LRFD Bridge Design Specifications, second ed., Washington DC, 1998.
[3] M.K. Tadros, N. Al-Omaishi, S.J. Seguirant, J.G. Gallt, Prestress losses in pretensioned high-strength concrete bridge girders, National cooperative highway research program report 496, Transportation Research Board, 2003. P. 73, ISBN: 0-309-08766-X.
[4] D.B. Garber, J.M. Gallardo, D.J. Deschenes, O. Bayrak, Experimental investigation of prestress losses in full-scale bridge girders, ACI Struct J 5 (2015) 553–564.
[5] F. Porco, A. Fiore, G. Porco, G. Uva, Monitoring and safety for prestressed bridge girders by SOFO sensors, J Civil Struct Health Monit 3 (2013) 3–18.
[6] Y.B. Lin, K.C. Chang, J.C. Chern, L.A. Wang, The health monitoring of a prestressed concrete beam by using fiber Bragg grating sensors, Smart Mats & Struct 13 (4) (2004) 712–718.
[7] K.H. Khayat., D. Mitchell, Self-consolidating concrete for precast, prestressed concrete bridge elements, National Cooperative Highway Research Program, NCHRP Report 628, Transportation Research Board, Washington DC, 2009. P. 73, ISBN: 0-309-08766-X.
[8] N. Gibbons, L.J. Butler, M. Williamson, A. Elwood, R. Platt, M. Henwood, J. Oliver, P. Holland, S. Dirar, S. Arthurs, C. Middleton, M. Elshafie, Monitoring the early age behaviour of prestressed concrete beams using fibre optic sensors, in: 16th European Bridge Conference and Exhibition, Edinburgh, June 2015.
[9] X.W. Ye, Y.H. Su, J.P. Han, Structural health monitoring of civil infrastructure using optical fiber sensing technology a comprehensive review, Sci. World J. (2014) 11, http://dx.doi.org/10.1155/2014/652329. 652329.
[10] R.Y. Chiao, C.H. Townes, B.P. Stoicheff, Stimulated Brillouin scattering and coherent generation of intense hypersonic waves, Phys. Rev. Lett. 12 (21) (1964) 592–595.
[11] M. Nikles, B.H. Vogel, F. Briffod, S. Grosswig, F. Sauser, S. Luebbecke, A. Bals, T. Pfeiffer, Leakage detection using fiber optics distributed temperature monitoring. in: Proc., 11th SPIE Annual Int. Symp. on Smart Structures and Materials, San Diego, 2004:18, doi:10.1117/12.540270.
[12] J.S. Selker, L. Thévenaz, H. Huwald, A. Mallet, W. Luxemburg, N. van de Giesen, M. Stejskal, J. Zeman, M. Westhoff, M.B. Parlange, Distributed fiber-optic temperature sensing for hydrologic systems, Water Resour. Res. 42 (W12202) (2006), http://dx.doi.org/10.1029/2006WR005326.
[13] P. Ferraro, G. De Natale, On the possible use of optical fiber Bragg gratings as strain sensors for geodynamical monitoring, Opt. Lasers Eng. 37 (2–3) (2002) 115–130, http://dx.doi.org/10.1016/S0143-8166(01)00141-5.
[14] H. Mohamad, Distributed optical fibre strain sensing of geotechnical structures (Ph.D. thesis), University of Cambridge, Cambridge, UK, 2008.

[15] X. Ning, H. Murayama, K. Kageyama, D. Wada, M. Kanai, I. Ohsawa, H. Igawa, Dynamic strain distribution measurement and crack detection of an adhesive-bonded single-lap joint under cyclic loading using embedded FBG, Smart Mater. Struct. 23 (10) (2014) 105011–105021, http://dx.doi.org/10.1088/0964-1726/23/10/105011.
[16] A. Bar-Cohen, B. Han, K.J. Kim, Thermo-optic effects in polymer Bragg gratings, in: Micro- and Opto-Electronic Materials and Structures: Physics, Mechanics, Design, Reliability, Packaging, E. Suhir, Y.C. Lee, C.P. Wong (Eds.), 2007, ISBN: 978-0-387-27974-9.
[17] M. Kreuzer, Strain Measurement with Fiber Bragg Grating Sensors, Technical Report HBM, Darmstadt Germany, 2011.
[18] C. Menn, Prestressed Concrete Bridges, Springer-Verlag, Vienna, 1990. P. 535.
[19] A.M. Neville, W.H. Dilger, J.J. Brooks, Creep of Plain and Structural Concrete, Construction Press, London, 1983. P. 361.
[20] T.K. Storm, S.H. Rizkalla, P.Z. Zia, Effects of production practices on camber of prestressed concrete bridge girders, PCI J. 58 (1) (2013) 96–111.
[21] P.J. Barr, B.M. Kukay, M.W. Halling, Comparison of prestress losses for a prestress concrete bridge made with high-performance concrete, J. Bridge Eng. 13 (5) (2008) 468–475.
[22] N. Yazdani, P. Mtenga, N. Richardson, Camber variation in precast girders, Conc. Intl. 21 (6) (1999) 45–49.
[23] K.M. Brown, Camber growth prediction in precast prestressed concrete bridge girders (PhD Dissertation). University of Idaho, 1998, p. 128.